Theory for linear and nonlinear planar Hall effect in topological insulator thin films

Wen Rao, Yong-Long Zhou, Yong-jia Wu, Hou-Jian Duan,* Ming-Xun Deng, and Rui-Qiang Wang†
Guangdong Provincial Key Laboratory of Quantum Engineering and Quantum Materials, School of Physics and Telecommunication Engineering, South China Normal University, Guangzhou 510006, China and Guangdong-Hong Kong Joint Laboratory of Quantum Matter, Frontier Research Institute for Physics, South China Normal University, Guangzhou 510006, China

(Received 9 January 2021; accepted 5 April 2021; published 16 April 2021)

Recently, the linear and nonlinear planar Hall effect (PHE) on the topological insulators (TIs) surface has been extensively studied in experiments. To explain this phenomenon, various microscopic mechanisms are proposed theoretically, and one has to employ different mechanisms to separately understand the linear and nonlinear PHE even for the same system. Here, we study the planar magnetic resistance effect in TI thin film and find that a peculiar anisotropic scattering and a spin valve structure with respect to the PHE can be caused by the tilt and shift of Dirac cones, respectively, which are induced by the combination of spin-momentum locking of surface states and an in-plane magnetic field. The tilt and shift effects can act as the origin of both the linear and nonlinear PHE by distorting the spin texture of surface states or forming the spin polarization. These two mechanisms interplay and dominate, respectively, in strong coupling (thin TI) and decoupling (thick TI) between bottom and top surfaces. For thick TI film, we show that both the linear and nonlinear PHEs induced by the tilt effect can recover the results observed in recent experiments. Our theory provides a perspective to understand the origin of both linear and nonlinear PHE observed in recent experiments.

DOI: 10.1103/PhysRevB.103.155415

I. INTRODUCTION

Planar Hall effect (PHE), manifesting itself as a detectable transverse voltage in response to a magnetic field applied in the plane of the sample and electric current, received great attention. It is very different from the ordinary Hall effect which, arising from the Lorentz force experienced by current carriers, requires the magnetic field to be perpendicular to both the electric current direction and the sample plane. The PHE is usually observed in ferromagnetic systems [1–3]. Interestingly, the PHE has also been verified experimentally in quite a few nonmagnetic topological materials, such as Weyl semimetals [4–8] and three-dimensional topological insulators (TIs) [9–11]. For these nonmagnetic materials, how to understand the origin of PHE is challenging. In Dirac and Weyl semimetals, recent theories [12–14] addressed that PHE is contributed by the chiral anomaly. The combination of the PHE with the negative longitudinal magnetoresistance is proposed to be a key transport signature of the chiral anomaly [15,16].

While the PHE phenomenon in Dirac/Weyl semimetals was well understood with the chiral anomaly, the origin of the PHE in TIs still remains unclear theoretically [17]. TIs are composed of fully insulating bulk states and metallic topological surface states [18–20]. One of the most fascinating properties in topological material is the spin-momentum locking of the helical topological surface states [21–25]. Experimentally, it has been confirmed that the linear [10,26–28] and nonlinear PHE [29–32] originates from surface states of TIs, but their microscopic mechanisms remain puzzled. Various mechanisms have been proposed for this phenomenon. For example, for the linear PHE, Taskin *et al.* employed a model of magnetic impurities to explain their experimental results [26], even though the $Bi_{2-x}Sb_xTe_3$ TI sample is in fact doped with nonmagnetic impurities. Akzyanov *et al.* [33] took the effect of hexagonal warping of TI surface states into account and obtained the transverse conductivity with $2\pi/3$ oscillation period, different from the experimentally observed π period. Nandy *et al.* [34] addressed that the nontrivial Berry phase and magnetic moments of bulk states may act as an origin of planar Hall response, but obviously it cannot be applicable to the above experiments with respect to TI surface states [11]. Very recently, our group found that the PHE can arise from the deformed dispersion of Dirac cones by an in-plane magnetic field, irrelevant to the magnetic nature of the scatterers [17]. For nonlinear PHE, He *et al.* ascribed it to the conversion of a nonequilibrium spin current into a charge current [29,30] and Dyrdal *et al.* to the spin-momentum-locking inhomogeneities [35]. Yasuda *et al.* regarded the asymmetric magnon scattering as a possible origin of nonlinear PHE in magnetic TIs [31,32]. Very recently, Yu *et al.* [36] theoretically found a nonlinear planar Nernst effect in nonmagnetic topological insulators, where the Nernst current is quadratically proportional to the temperature gradient and linearly proportional to the in-plane magnetic field.

In this paper, we study the origin of both the linear and nonlinear PHE on a TI surface. In our previous work [17],

*dhjphd@163.com
†wangruiqiang@m.scnu.edu.cn

we find that the tilt of the Dirac cone can lead to the linear PHE for a single TI surface. In this paper, we extend the discussions to the nonlinear PHE and find that for thick TI film where top-bottom surfaces are uncoupled, the tilt effect not only causes the linear PHE but also the nonliear PHE, with the B and θ_B dependence being in good agreement with recent experiments for linear PHE [10,26–28] and nonlinear PHE [29,30]. Usually, one has to employ different mechanisms to separately understand the linear and nonlinear PHE even for the same system. For example, in recent experiments [29,30], the nonlinear magnetic resistance is attributed to the warping effect but it fails to explain the linear PHE [33]. Furthermore, we extend our discussions to the thin film with hybridization between the top and bottom helical surface states [37], which is experimentally adopted to reduce the disturb from bulk conductivity. We find that relative shift between the cones of the top and bottom surfaces, induced by an applied in-plane magnetic field, also can act as an origin of the linear PHE, which dominates in the strong coupling between top-bottom surfaces. For thin TI film with strong coupling, the contributions from two surfaces have opposite sign with the same amplitude and compensate each other owing to the opposite spin texture and the odd function of $\mathbf{B}$. Nevertheless, the nonlinear PHE also can emerge if one exerts a dual-gate voltage to generate different chemical potentials between two surfaces, where two mechanisms would compete with each other, exhibiting rich dependence on the angle and magnitude of the magnetic field.

II. MODEL AND PHE MECHANISMS

Considering a TI thin film subjected to an external in-plane magnetic field $\mathbf{B} = B[\cos(\theta_B), \sin(\theta_B)]$, the disturbed helical surface states can be described by a low-energy Hamiltonian $H_{\rm TI} = \sum_{\mathbf{k}} c^{\dagger}_{\mathbf{k}} h_{TI}(\mathbf{k}) c_{\mathbf{k}}$ with

$$h_{\rm TI} = \varepsilon_0(\mathbf{k}) + \tau_z \hbar v_F (\mathbf{k} \times \sigma)_z + \tau_x \sigma_0 \Delta + \tau_0 (\mathbf{B} \cdot \sigma). \quad (1)$$

Here, $c^{\dagger}_{\mathbf{k}} = (c^{\dagger}_{\mathbf{k}\uparrow}, c^{\dagger}_{\mathbf{k}\downarrow})$ is the creation operator of electrons with wave vector $\mathbf{k} = k[\cos(\theta_k), \sin(\theta_k)]$, v_F represents the Fermi velocity, and σ and τ are the Pauli matrices, acting on the electron spin space and the top and bottom surfaces, respectively. Δ describes the hybridization strength between top and bottom surface states as the thickness of the film is comparable to the "penetration depth" of the surface states into the bulk [38]. It typically happens at a thickness of five to ten quintuple layers [39,40]. The higher-order term $\varepsilon_0(\mathbf{k}) = D\mathbf{k}^2$ in TIs can stem from the asymmetry between the electron and hole bands [41–43]. Diagonalizing the Hamiltonian of Eq. (1), the resulting dispersion reads as ($\hbar v_F = 1$)

$$\varepsilon^s_{\zeta} = \varepsilon_0(\mathbf{k}) + s\sqrt{B^2 + k^2 + \Delta^2 + 2\zeta\alpha}, \quad (2)$$

where $\alpha = [(\mathbf{k} \times \mathbf{B})^2_z + B^2\Delta^2]^{1/2}$, $s = \pm$ denotes the conduction and valence bands, respectively, and $\zeta = \pm 1$ describes the splitting of bands induced by Δ. The corresponding eigenstates $\psi^s_{\zeta}(\mathbf{k})$ can also be solved as

$$\psi^s_{\zeta}(\mathbf{k}) = \frac{\sqrt{\alpha + \zeta(\mathbf{k} \times \mathbf{B})_z}}{2\Delta\sqrt{\alpha}/s\varepsilon_{\zeta}} \begin{pmatrix} [\zeta\alpha - (\mathbf{k} \times \mathbf{B})_z]/(s\varepsilon_{\zeta} B e^{i\theta_B}) \\ [\alpha - s\zeta(\mathbf{k} \times \mathbf{B})_z]/(\alpha + \zeta\beta) \\ \zeta\Delta B e^{-i\theta_B}/(\alpha + \zeta\beta) \\ \Delta/s\varepsilon_{\zeta} \end{pmatrix}, \quad (3)$$

with $\beta = B^2 + i\mathbf{k} \cdot \mathbf{B}$ and $\varepsilon_{\zeta} = [B^2 + k^2 + \Delta^2 + 2\zeta\alpha]^{1/2}$.

With respect to the PHE, we would concentrate on the influence of an in-plane magnetic field $\mathbf{B}$. It is noted that $\mathbf{B}$ has two effects: (i) leads to the tilt of the Dirac cone; (ii) shifts the positions of the two Dirac cones to opposite direction, i.e., $(0, 0) \rightarrow \pm B[-\sin(\theta_B), \cos(\theta_B)]$ for top and bottom surfaces, respectively. In order to clarify the former, we expand the Hamiltonian ($\Delta = 0$) of Eq. (1) around the shifted Dirac point $\pm B[-\sin(\theta_B), \cos(\theta_B)]$ in momentum $\mathbf{k}$. When defining the momentum $\mathbf{k}'$ measuring from the shifted Dirac point, the Zeeman term is canceled but accompanied by a term $\pm 2\tau_z DB(k'_y \cos\theta_B - k'_x \sin\theta_B)$. Obviously, this term tilts the pristine upright Dirac cone due to the broken Lorentz invariance.

Both effects of the in-plane magnetic field are expected to cause the PHE. Before carrying out the numerical calculations, we understand the origin of the PHE physically. (i) Tilt effect. To clarify it, we choose two disconnected Dirac cones with $\Delta = 0$ where the shift effect plays no effect. The in-plane magnetic field tilts the Dirac cone, which deforms the circular Fermi surface to an elliptic one, as shown in Fig. 1(a). As a result, the spins of states $|\mathbf{k}\rangle$ and $|-\mathbf{k}\rangle$ along the field direction (y axis) are no longer antiparallel [Fig. 1(b)], lifting the prohibition of spin-flip backscattering, while in the direction perpendicular to $\mathbf{B}$, the backscattering is still prohibited. This is confirmed by calculating the momentum-dependent spin texture $s(\mathbf{k}) = \langle\psi^+_-(\mathbf{k})|\sigma|\psi^+_-(\mathbf{k})\rangle$ and the dependence of $\hat{\mathbf{k}} \cdot \hat{\mathbf{s}} = \mathbf{k} \cdot \mathbf{s}/(|\mathbf{k}||\mathbf{s}|)$ on $\theta_{\mathbf{k}}$ (the angle of $\mathbf{k}$) is plotted in Fig. 1(c). Obviously, the nonzero value implies that the spin-momentum locking is violated, especially along the field direction $\theta_{\mathbf{k}} = (n + 1/2)\pi$, but it remains zero in the direction perpendicular to $\mathbf{B}$. The anisotropic spin texture results in the PHE.

(ii) Shift effect. When an in-plane magnetic field is applied, two Dirac cones would shift in the opposite direction, perpendicular to $\mathbf{B}$ as shown in Fig. 1(d). Partly overlapping between two Dirac cones leads to a net spin polarization parallel to the magnetic field as indicated in the right of Fig. 1(e). We calculate the net spin polarization $\mathbf{S} = \int \mathbf{s}(\mathbf{k}) d\mathbf{k}$ with the Fermi energy ε_F located in the valence band and plot the result in Fig. 1(f) (indicated by the bold red arrow). As a consequence, there forms a spin valve structure between the current-induced spin (indicated by red thin solid arrow) of Dirac electrons due to the spin-momentum locking and the net spin $\mathbf{S}$. When the current direction is perpendicular to $\mathbf{B}$, the electron spin is always antiparallel to $\mathbf{S}$, whose antiparallel spin valve prohibits the electron back transport through inter-surface coupling [low resistivity (LR) states of Fig. 1(e)] and decreases the resistivity but has less influence for the current following along the $\mathbf{B}$ direction [high resistivity (HR) states of Fig. 1(e)]. Naturally, this anisotropy of spin transport can in turn lead to the transverse PHE.

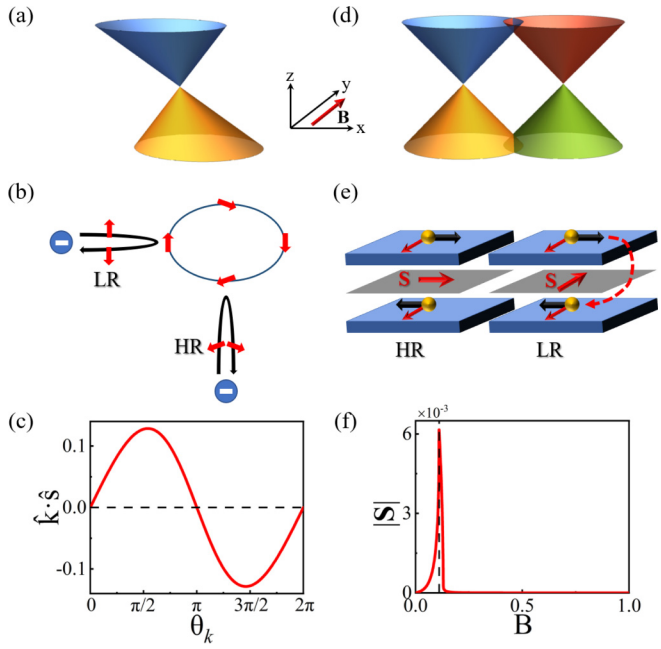

FIG. 1. Dirac cones of top and bottom surfaces in TI thin films with (a) tilt effect and (d) shift effect induced by the in-plane magnetic field **B**. Schematic pictures of (b) electron scattering with tilt effect and (e) spin valve structure with shift effect. Both cases exhibit a high resistivity state when the incident direction of electrons are parallel to the **B**. The red and black solid arrows stand for the spin and incident directions of Dirac electrons, respectively. HR (LR) stands for high (low) resistivity states. (c) θ_k -dependent spin texture $\hat{\mathbf{k}}\cdot\hat{\mathbf{s}}$ with $D = 0.2$, $\Delta = 0$, and $B = 0.3$. (f) B-dependent net spin polarization $|\mathbf{S}|$ with $\Delta = 0.01$ and $D = 0$. In (c) and (f), finite Fermi energy $\varepsilon_F = -0.12$ ($\hbar v_F = 1$) is set.

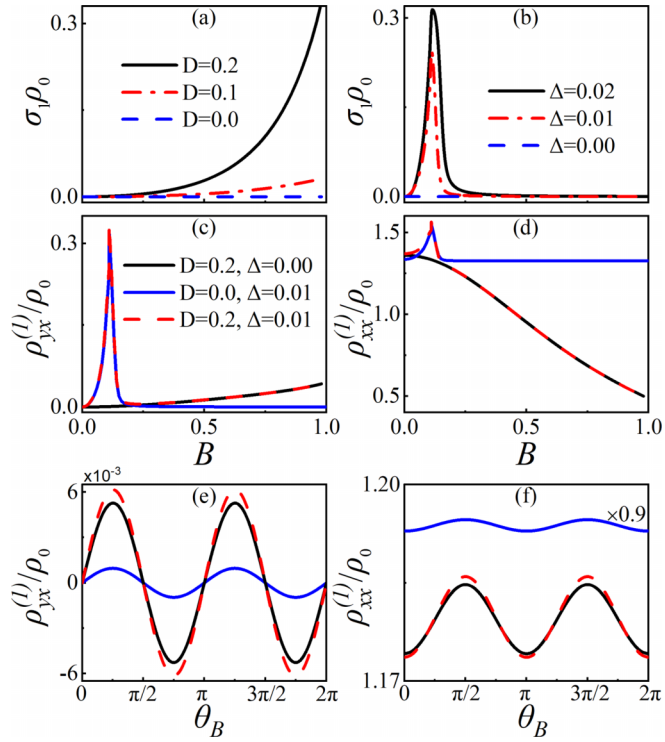

FIG. 2. The dependence of the PHC amplitude σ_1 on the magnetic field strength B with (a) only tilt effect and (b) only shift effect. The dependence of (c) the PHR $\rho_{yx}^{(1)}$ and (d) AMR $\rho_{xx}^{(1)}$ on B, where $\theta_B = \pi/4$. The angular θ_B dependence of (e) PHR $\rho_{yx}^{(1)}$ and (f) AMR $\rho_{xx}^{(1)}$, where $B = 0.3$. In all panels, other parameters are set as $\varepsilon_F = -0.12$ and $\hbar v_F = 1$, and we denote $\rho_0 = 2\pi h/e^2\gamma$.

For the convenience of analysis, in the following calculation, we employ the quasiclassical Boltzmann transport equation to calculate the electronic contribution to the planar Hall conductivity (PHC) and anisotropic magnetic conductivity (AMC). In the steady state, the Boltzmann transport equation [44] is expressed as

$$-\frac{eE_x}{\hbar}\frac{\partial f_{\mathbf{k}}}{\partial k_x} = -\frac{f_{\mathbf{k}} - f_{\rm eq}}{\gamma(\mathbf{k})}, \tag{4}$$

where we use the relaxation time approximation $\gamma(\mathbf{k}) = \gamma$ for simplicity. $f_{\rm eq}$ is the equilibrium Fermi-Dirac distribution function in the absence of external fields. When an external electric field $\mathbf{E} = E_x\hat{x}$ is applied along the x direction, the resulting distribution function $f_{\mathbf{k}}$ is shifted and it can be expanded in the electric field E_x as $f_{\mathbf{k}} = f_{\rm eq} + \delta f_{\mathbf{k}}^{(1)} + \delta f_{\mathbf{k}}^{(2)} + \cdots$.

III. LINEAR PHE

In reality, the tilt and shift coexist simultaneously and interplay with each other. Up to the first order term of E_x, from Eq. (4) we obtain

$$\delta f_{\mathbf{k}}^{(1)} = \frac{e\gamma}{\hbar}E_x\frac{\partial f_{\rm eq}}{\partial k_x}, \tag{5}$$

and the current density can be calculated via $J_{e,i} = -e\int\frac{d^2\mathbf{k}}{(2\pi)^2}v_i\delta f_{\mathbf{k}}^{(1)}$, where v_i is the group velocity along the i direction. Thus, the conductivity tensor can be obtained as

$$\sigma_{ix}^{(1)} = -\frac{e^2\gamma}{\hbar}\int\frac{d^2\mathbf{k}}{(2\pi)^2}v_i v_x\frac{\partial f_{\rm eq}}{\partial\varepsilon}. \tag{6}$$

For convenience, we rotate the coordinate system of $(k_\parallel, k_\perp)^T = \hat{R}(k_x, k_y)^T$ and $(v_\parallel, v_\perp)^T = \hat{R}(v_x, v_y)^T$ with T the transpose and the rotation matrix $\hat{R}$ given by $\hat{R} = \begin{pmatrix}\cos(\theta_B) & \sin(\theta_B)\\ -\sin(\theta_B) & \cos(\theta_B)\end{pmatrix}$ where $\parallel$ ($\perp$) is parallel and perpendicular to **B**. We arrive at the expression for the conductivity tensors (see the Supplementary Material [45])

$$\begin{aligned}\sigma_{yx}^{(1)} &= \sigma_1\cos(\theta_B)\sin(\theta_B),\\ \sigma_{xx}^{(1)} &= \sigma_0 + \sigma_1\cos^2(\theta_B),\end{aligned} \tag{7}$$

with

$$\begin{aligned}\sigma_1 &= -\frac{e^2\gamma}{\hbar}\int\frac{d^2\mathbf{k}}{(2\pi)^2}(v_\parallel^2 - v_\perp^2)\frac{\partial f_{\rm eq}}{\partial\varepsilon},\\ \sigma_0 &= -\frac{e^2\gamma}{\hbar}\int\frac{d^2\mathbf{k}}{(2\pi)^2}v_\perp^2\frac{\partial f_{\rm eq}}{\partial\varepsilon}.\end{aligned} \tag{8}$$

In the above equations, we have dropped the integral with respect to $v_\parallel v_\perp$, which vanishes due to $v_\parallel = (2D - s/\varepsilon_\zeta)k_\parallel$, the odd function of $k_\parallel$.

We plot the dependence of the PHC amplitude σ_1 on the magnetic field strength B in Fig. 2(a) for different D with $\Delta = 0$ and in Fig. 2(b) for different Δ with $D = 0$. Both figures show the finite PHC. In Fig. 2(a), with the increase of

B, the tilt effect of the Dirac cone becomes prominent and the anisotropy of scattering enhances the PHC, whose amplitude is $\sigma_1 \propto B^2$ (see analytical results in Supplemental Material [45]), in agreement with the recent experiment [10,26,28]. With only the shift effect as in Fig. 2(b), the PHC increases first and then decreases to zero, nonmonotonously dependent on B. This nonmonotonous behavior stems from the net spin polarization $\mathbf{S}$ in Fig. 1(f). The peak of the PHC amplitude σ_1 is approximately located at $B = \Delta + \varepsilon_F$. The size of the Fermi surface will increase with B until a critical value $B = \Delta + \varepsilon_F$ where two circular Fermi surfaces are just separated. It is emphasized that in the regime of vanished $\mathbf{S}$, the transport becomes isotropic and so the PHE vanishes, which implies the existence of $\mathbf{S}$ is decisive for the formation of PHE. According to Eq. (7), the nonzero σ_1 would cause the PHC $\sigma_{xy}^{(1)}$ and the AMC $\sigma_{xx}^{(1)}$, along with oscillations following the typical angular dependence of $\sin(\theta_B)\cos(\theta_B)$ and $\cos^2(\theta_B)$, respectively. Different from the conventional Hall effect which satisfies the antisymmetry property, the PHC $\sigma_{xy}^{(1)}$ is symmetric with respect to the magnetic field.

In a realistic system, both mechanisms coexist. In Figs. 2(c) and 2(d), we plot the dependence of the planar Hall resistivity (PHR) $\rho_{xy}^{(1)}$ and anisotropic magnetic resistivity (AMR) $\rho_{xx}^{(1)}$ on B, which can be obtained with $\rho_{ix}^{(1)} = \sigma_{ix}^{(1)}/(\sigma_{xx}^{(1)2} + \sigma_{yx}^{(1)2})$. For comparison, the case with only tilt or with only shift is also shown. It is found that the two effects would compete with each other, respectively dominating in the different region of the magnetic field strength B. We fix the parameter D and tune the coupling strength Δ, which characterizes the change of TI thickness. For thick TI with $\Delta = 0$, $\rho_{xy}^{(1)}$ increases proportional to B^2, which dominates for large B and becomes unsaturated. With the reduced thickness or increasing Δ, while the $\rho_{xy}^{(1)}$ in large B remains almost unchanged, in the region of low B there emerges a peak. The emerging peak of the PHE is ascribed to the contribution from shift effect and reflected in the net spin polarization $\mathbf{S}$ [Fig. 1(f)]. A similar scenario exists for AMR $\rho_{xx}^{(1)}$ as well. The nonmonotonous behavior has been reported experimentally in TI thin film [27]. Besides, we find that $\rho_{yx}^{(1)}$ and $\rho_{xx}^{(1)}$ oscillate with a period of π as a function of θ_B, as illustrated in Figs. 2(e) and 2(f). The oscillating behavior has recently been observed experimentally [26,27,29]. These PHEs emerge either from the tilt-distorted Fermi surface or from the shift-induced net spin by in-plane magnetic field, whose mechanisms are new, different from the previous theories [46,47], where the spin flip originates from scattering off magnetic impurities.

IV. NONLINEAR PHE

When the proposed tilt and shift mechanisms can be applied to explain the linear PHE, we tend to explore their roles in nonlinear PHE observed in recent experiments [29,30] since both the linear and nonlinear PHEs are detected in a similar TI system. Since the PHE appears only when the Fermi level lies in the conduction (valence) band above (below) the Dirac point, the contribution from the Berry curvature can be ignored. Expanding the nonequilibrium distribution function in Eq. (4) up to the second order of E_x, one obtains

$$\delta f_{\mathbf{k}}^{(2)} = \frac{e\gamma}{\hbar} E_x \frac{\partial f_{\mathbf{k}}^{(1)}}{\partial k_x}, \tag{9}$$

and the corresponding longitudinal and transversal conductivities read (see Supplemental Material [45])

$$\sigma_{ix}^{(2)} = \frac{e^3\gamma^2 E_x}{(2\pi)^2\hbar^2} \int d^2\mathbf{k} \frac{\partial v_i}{\partial k_x} v_x \frac{\partial f_{\mathrm{eq}}}{\partial \varepsilon}. \tag{10}$$

At low temperatures, the presence of the function $\partial f_{\mathrm{eq}}/\partial\varepsilon$ guarantees that only states on the Fermi surface will contribute to the integral. Compared with linear conductivity of Eq. (6), the main change is that v_i is replaced with $\partial v_i/\partial k_x$. Notice that this replacement is not trivial since it can change the even-odd function of the integrand, which is critical for the appearance of finite $\sigma_{ix}^{(2)}$. For example, for the linear case, the integral in Eq. (8) with respect to the crossed term $v_\parallel v_\perp$ vanishes due to the odd function of $k_\parallel$. By contrast, in the nonlinear conductivity of Eq. (10), the crossed term $\frac{\partial v_\perp}{\partial k_\parallel} v_\parallel$ does not vanish but plays a determined role in the integral over $\mathbf{k}$. This implies that Eq. (10) has different physics from Eq. (6).

With the conductivities from Eqs. (6) and (10), we can calculate the corresponding PHR ρ_{yx} and AMR ρ_{xx} using [29,30]

$$\begin{aligned} \rho_{xx} &= \hat{\mathbf{z}} \cdot (\mathbf{E} \times \mathbf{J})/|\mathbf{J}|^2, \\ \rho_{yx} &= \mathbf{E} \cdot \mathbf{J}/|\mathbf{J}|^2. \end{aligned} \tag{11}$$

Here, $\mathbf{E} = (E_x, 0)$ and $\mathbf{J} = \mathbf{J}^{(1)} + \mathbf{J}^{(2)} + \cdots$ is the total current density with the superscripts (1) and (2) denoting for linear and nonlinear contributions, respectively.

A. The nonlinear PHE contributed by only tilt effect

First, we consider the case with only tilt effect ($D \neq 0$, $\Delta = 0$), corresponding to the experiment setup with thick TI [29,30]. In this situation, the transversal conductivity $\sigma_{yx}^{(2)}$ is contributed to by a single surface. As before, we rotate the original coordinate system (k_x, k_y) to be a new one $(k_\parallel, k_\perp)$ using the matrix $\hat{R}$, and the partial differential $\partial v_i/\partial k_x$ can be rewritten as

$$\frac{\partial v_i}{\partial k_x} = \frac{\partial v_i}{\partial k_\parallel}\cos(\theta_B) - \frac{\partial v_i}{\partial k_\perp}\sin(\theta_B). \tag{12}$$

Inserting it into Eq. (10) and performing the integrating over $\mathbf{k}$, only the terms related to $\frac{\partial v_\perp}{\partial k_\parallel} v_\parallel$ and $(\frac{\partial v_\perp}{\partial k_\perp} - \frac{\partial v_\parallel}{\partial k_\parallel}) v_\perp$ survive since the other terms are the odd functions of $k_\parallel$. Thus, at low temperatures, $\sigma_{yx}^{(2)}$ can be simplified as

$$\begin{aligned} \sigma_{yx}^{(2)} = -\frac{e^3\gamma^2 E_x}{(2\pi)^2\hbar^2} \int d\mathbf{k} \cos(\theta_B)\delta(\varepsilon^- - \varepsilon_F) \\ \times \left[\frac{\partial v_\perp}{\partial k_\parallel} v_\parallel \cos(2\theta_B) + \left(\frac{\partial v_\perp}{\partial k_\perp} - \frac{\partial v_\parallel}{\partial k_\parallel}\right) v_\perp \sin^2(\theta_B)\right]. \end{aligned} \tag{13}$$

With Eq. (11), we can calculate $\rho_{yx}^{(2)}$ and $\rho_{xx}^{(2)}$ and present the corresponding numerical results in Fig. 3. In Figs. 3(a) and 3(b), we depict the dependence on the magnetic field direction θ_B of nonlinear PHR $\rho_{yx}^{(2)}$ and nonlinear AMR $\rho_{xx}^{(2)}$. The most prominent characteristic is that $\rho_{yx}^{(2)}$ behaves as $\cos(\theta_B)$ and $\rho_{xx}^{(2)}$ as $\sin(\theta_B)$, both of which oscillate with a period of 2π. This is greatly distinguished from the linear case shown in

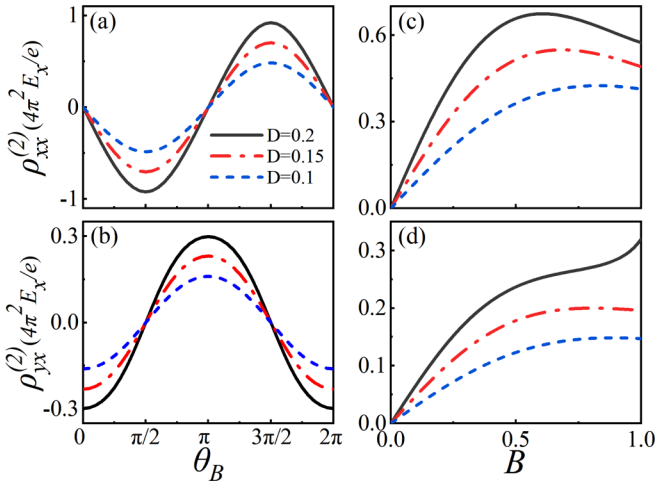

FIG. 3. The dependence of the nonlinear PHR on (a),(b) the angular θ_B and (c),(d) the field strength B for a single TI surface ($\Delta = 0$) for different tilt parameters D. Other parameters are set as $\varepsilon_F = -0.2$, (a),(b) $B = 0.45$ and (c),(d) $\theta_B = 5\pi/4$.

Fig. 2, where the magnetic resistivity exhibits a period of π. At the same time, for low magnetic field B, both $\rho_{yx}^{(2)}$ and AMR $\rho_{xx}^{(2)}$ are proportional to B, rather than to B^2 in the linear case. These results recover the bilinear behavior as observed in recent experiments [29,30], where the authors attributed the bilinear magnetoelectric resistivity to the warping effect. Notice the warping effect cannot explain the linear PHE since it only leads to the transverse conductivity with $2\pi/3$ oscillation period [33], thus the linear and nonlinear PHEs in experiments [29,48] are attributed to different mechanisms. Instead, we here find that both the linear and nonlinear PHEs can be attributed to the same mechanism, the field-induced tilt of the Dirac cone.

In order to see it more clearly, we further derivate the analytic expressions. Expanding the integrand of Eq. (10) to the leading order of B and setting $\varepsilon_F < 0$, we can express $\sigma_{yx}^{(2)}$ as (see Supplemental Material [45])

$$\sigma_{yx}^{(2)} \approx -\frac{e^3\gamma^2 E_x B\cos(\theta_B)}{(2\pi)^2\hbar^2}\int d\mathbf{k}\frac{\partial v_\perp}{\partial k_\parallel}v_\parallel\left[\frac{d\delta(\varepsilon^- - \varepsilon_F)}{dB}\right]_{B=0},$$
$$= \frac{e^3\gamma^2 D E_x}{4\pi\hbar^2(1+4\varepsilon_F D)}B\cos(\theta_B). \tag{14}$$

From the above equation, we find that the nonzero $\sigma_{yx}^{(2)}$ is completely determined by the Delta function $\delta(\varepsilon^- - \varepsilon_F)$ or the parity of the energy band ε^-, due to the even function $\frac{\partial v_\perp}{\partial k_\parallel}v_\parallel$ of $\mathbf{k}$. In the presence of the tilt effect, nonzero $\sigma_{yx}^{(2)}$ appears, which is induced by the broken parity of the energy ε^-, i.e., $\varepsilon^-(\mathbf{k}) \neq \varepsilon^-(-\mathbf{k})$. Similar to the calculation process of $\sigma_{yx}^{(2)}$, one can obtain the longitudinal conductivity $\sigma_{xx}^{(2)}$, which is given by

$$\sigma_{xx}^{(2)} \approx -\frac{e^3\gamma^2 D E_x C_x}{4\pi\hbar^2(1+4D\varepsilon_F)^{3/2}}B\sin(\theta_B), \tag{15}$$

with $C_x = 4 + 16\varepsilon_F D + (15 + 48\varepsilon_F D)\sqrt{1+4D\varepsilon_F}$. Substituting the result of $\sigma_{ix}^{(1)}$ and $\sigma_{ix}^{(2)}$ into Eq. (11) and remaining up to the first order of E_x and B, one can obtain the nonlinear PHR $\rho_{yx}^{(2)}$ and the nonlinear AMR $\rho_{xx}^{(2)}$

$$\rho_{yx}^{(2)} \propto E_x DB\cos(\theta_B),$$
$$\rho_{xx}^{(2)} \propto E_x DB\sin(\theta_B). \tag{16}$$

These analytical expressions agree well with the numerical results presented in Fig. 3.

B. The nonlinear PHE contributed by coexistence of tilt and shift effects

Above discussions are suitable only for the thick film as in experiments [29,30]. For the thin TI film, the coupling ($\Delta \neq 0$) is included in addition. For this situation with $D \neq 0$ and $\Delta \neq 0$, using the rotational matrix $\hat{R}$, the nonlinear conductivity $\sigma_{yx}^{(2)}$ in Eq. (10) can be expressed as

$$\sigma_{yx}^{(2)} = \frac{e^3\gamma^2 E_x}{(2\pi)^2\hbar^2}\int d\mathbf{k}\frac{\partial f_{\rm eq}}{\partial\varepsilon}\left[\frac{v_\parallel\partial v_\perp/\partial k_\parallel}{\sec(\theta_B)} - \frac{v_\perp\partial v_\perp/\partial k_\parallel}{\csc(\theta_B)}\right]$$
$$\times\cos(2\theta_B)$$
$$+\frac{e^3\gamma^2 E_x}{(2\pi)^2\hbar^2}\int d\mathbf{k}\frac{\partial f_{\rm eq}}{\partial\varepsilon}\left(\frac{\partial v_\parallel}{\partial k_\parallel} - \frac{\partial v_\perp}{\partial k_\perp}\right)v_\parallel\frac{\sin(2\theta_B)}{2\sec(\theta_B)}$$
$$-\frac{e^3\gamma^2 E_x}{(2\pi)^2\hbar^2}\int d\mathbf{k}\frac{\partial f_{\rm eq}}{\partial\varepsilon}\left(\frac{\partial v_\parallel}{\partial k_\parallel} - \frac{\partial v_\perp}{\partial k_\perp}\right)v_\perp\frac{\sin(2\theta_B)}{2\csc(\theta_B)}. \tag{17}$$

Note that all the terms with respect to the velocity in Eq. (17) are the odd function of $k_\parallel$ or $k_\perp$ (see Supplemental Material [45]), and thus nonlinear response is tightly related to the parity of $\frac{\partial f_{\rm eq}}{\partial\varepsilon}$, i.e, the parity of the energy band ε_ζ^s. For symmetric Fermi energy between the top and bottom surfaces, one can find that ε_ζ^s is the even function of $\mathbf{k}$, i.e., $\varepsilon_\zeta^s(\mathbf{k}) = \varepsilon_\zeta^s(-\mathbf{k})$, which would contribute a vanished nonlinear conductivity. Physically, the opposite spin textures in top and bottom surfaces have an opposite response to $\mathbf{B}$ since the nonlinear PHR and AMR are the odd function of $\mathbf{B}$. Consequently, the contributions from top and bottom surfaces have opposite sign with the same amplitude and compensate each other once two surfaces are coupled in TI thin films.

To observe the nonlinear effect in thin TI film, one can apply a dual-gate voltage to control the chemical potential $V\tau_z$ of the top and bottom surfaces independently, which is extensively adopted in experiments [26,49,50]. Thus, the parity of the energy band ε_ζ^s is destroyed, i.e., $\varepsilon_\zeta^s(-\mathbf{k}) \neq \pm\varepsilon_\zeta^s(\mathbf{k})$, leading to nonzero magnetic resistivity. As a result, the finite nonlinear $\rho_{yx}^{(2)}$ and $\rho_{xx}^{(2)}$ appear. In Figs. 4(a) and 4(b), we illustrate the angular dependence of the nonlinear PHR $\rho_{yx}^{(2)}$ and nonlineaer AMR $\rho_{xx}^{(2)}$, respectively, for different values of D and Δ. For the thin TI film with asymmetric chemical potential, both the tilt and shift effects attribute to nonlinear response. In Fig. 4, for thin TI film with asymmetric chemical potential with $\Delta = 0$, the nonlinear resistivity behaves as the case of a single surface in Fig. 3. Once the coupling is included, the complex angular dependence contributed by the shift effect competes with the tilt effect, leading to neither cosine nor sine function. Even so, the total curve still remains a 2π-periodic oscillation. For this scenario, as far

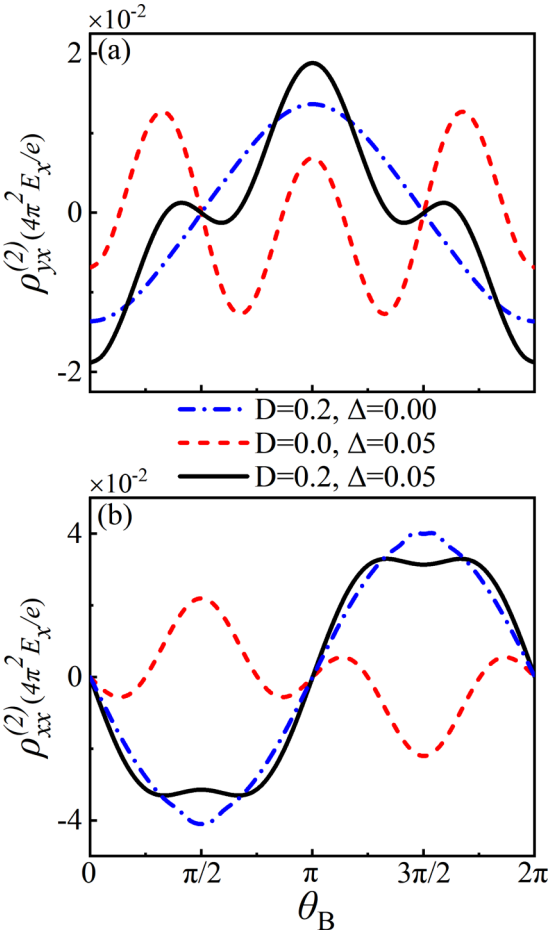

FIG. 4. The angular dependence of the nonlinear (a) PHR $\rho^{(2)}_{yx}$ and (b) AMR $\rho^{(2)}_{xx}$ for different values of D and Δ. Other parameters are fixed as $\varepsilon_F = -0.2$, $B = 0.45$, and $V = 0.15$.

as we know, there is no experimental report, which is expected to be tested in further experiments.

V. REMARKS AND CONCLUSION

The tilt effect is not limited to the electron-hole anisotropy but also arises for any high-order momentum terms $\mathbf{k}^n$. As an in-plane magnetic field is exerted, $\mathbf{k}^n$ can be expanded around the shifted Dirac point $(\mathbf{k} - \mathbf{B})^n$. As a result, a term $\mathbf{k} \cdot \mathbf{B}$ is always generated, which tilts the linear Dirac cone $\hbar v_F(\mathbf{k} \times \sigma)_z$. Thus, the tilt effect exists extensively.

We have explored both the linear and nonlinear planar magnetic resistance effect when an in-plane magnetic field $\mathbf{B}$ is applied in TI thin films with hybridization between the opposite helical surfaces. We find that PHE can emerge on the TI surfaces even in the absence of magnetic impurities. We proposed two mechanisms related to the PHE: tilt and the relative shift effect of Dirac cones, induced by an applied in-plane magnetic field. The former generates the anisotropic backscattering due to the distorting spin texture of surface states and the latter is due to the nonzero net spin polarization. We find that for thick TI film where top-bottom surfaces are uncoupled, the tilt effect not only causes the linear PHE but also the nonliear PHE, with the B and θ_B dependence being in good agreement with recent experiments for linear PHE [10,26–28] and nonlinear PHE [29,30]. Notice that in recent experiments [29,30], the nonlinear magnetic resistance is attributed to the warping effect but it fails to explain the linear PHE [33]. Here, we attribute both the nonlinear and linear response to the same tilt mechanism. For thin TI film with strong coupling between top-bottom surfaces, the contributions from two surfaces have opposite sign with the same amplitude and compensate each other owing to the opposite spin texture and the odd function of $\mathbf{B}$. Nevertheless, this compensation can be lifted if we exert a dual-gate voltage to generate different chemical potentials between two surfaces. As a consequence, the nonlinear PHE emerge and two mechanisms would compete with each other. This in turn leads to a complex angular dependence but still remaining a 2π-periodic oscillation, which is expected to be verified in further experiments.

ACKNOWLEDGMENTS

This work was supported by GDUPS (2017), by the Science and Technology Program of Guangzhou (No. 2019050001), by the National Natural Science Foundation of China (Grants No. 11874016 and No. 11904107), by the Guangdong NSF of China (Grants No. 2021A1515011566 and No. 2020A1515011566), and by the Project funded by the China Postdoctoral Science Foundation (Grant No. 2020M672666).

W.R. and Y.-L.Z. contributed equally to this work.

[1] H.-X. Tang, R. K. Kawakami, D. D. Awschalom, and M. L. Roukes, Phys. Rev. Lett. **90**, 107201 (2003).

[2] K. M. Seemann, F. Freimuth, H. Zhang, S. Blügel, Y. Mokrousov, D. E. Bürgler, and C. M. Schneider, Phys. Rev. Lett. **107**, 086603 (2011).

[3] M. Bowen, K. J. Friedland, J. Herfort, H. P. Schönherr, and K. H. Ploog, Phys. Rev. B **71**, 172401 (2005).

[4] M. Wu, G. Zheng, W. Chu, Y. Liu, W. Gao, H. Zhang, J. Lu, Y. Han, J. Zhou, W. Ning, and M. Tian, Phys. Rev. B **98**, 161110(R) (2018).

[5] P. Li, C.-H. Zhang, J.-W. Zhang, Y. Wen, and X.-X. Zhang, Phys. Rev. B **98**, 121108(R) (2018).

[6] R. Singha, S. Roy, A. Pariari, B. Satpati, and P. Mandal, Phys. Rev. B **98**, 081103(R) (2018).

[7] N. Kumar, S. N. Guin, C. Felser, and C. Shekhar, Phys. Rev. B **98**, 041103(R) (2018).

[8] H. Li, H.-W. Wang, H.-T. He, J.-N. Wang, and S.-Q. Shen, Phys. Rev. B **97**, 201110(R) (2018).

[9] O. Breunig, Z. Wang, A. A. Taskin, J. Lux, A. Rosch, and Y. Ando, Nat. Commun. **8**, 15545 (2017).

[10] B. Wu, X.-C. Pan, W. Wu, F. Fei, B. Chen, Q. Liu, H. Bu, L. Cao, F. Song, and B. Wang, Appl. Phys. Lett. **113**, 011902 (2018).

[11] D. Rakhmilevich, F. Wang, W.-W. Zhao, M. H. W. Chan, J. S. Moodera, C.-X. Liu, and C.-Z. Chang, Phys. Rev. B **98**, 094404 (2018).

[12] A. A. Burkov, Phys. Rev. B **96**, 041110(R) (2017).

[13] S. Nandy, G. Sharma, A. Taraphder, and S. Tewari, Phys. Rev. Lett. **119**, 176804 (2017).

[14] M.-X. Deng, H.-J. Duan, W. Luo, W.-Y. Deng, R.-Q. Wang, and L. Sheng, Phys. Rev. B **99**, 165146 (2019).

[15] A. A. Burkov, Phys. Rev. B **91**, 245157 (2015).

[16] T. Liang, J. Lin, Q. Gibson, S. Kushwaha, M. Liu, W. Wang, H. Xiong, J. A. Sobota, M. Hashimoto, P. S. Kirchmann, Z.-X. Shen, R. J. Cava, and N. P. Ong, Nat. Phys. **14**, 451 (2018).

[17] S.-H. Zheng, H.-J. Duan, J.-K. Wang, J.-Y. Li, M.-X. Deng, and R.-Q. Wang, Phys. Rev. B **101**, 041408(R) (2020).

[18] J. E. Moore, Nature (London) **464**, 194 (2010).

[19] X.-L. Qi and S.-C. Zhang, Phys. Today **63**, 33 (2010).

[20] M. Z. Hasan and C. L. Kane, Rev. Mod. Phys. **82**, 3045 (2010).

[21] Y. Ando, J. Phys. Soc. Jpn. **82**, 102001 (2013).

[22] C. L. Kane and E. J. Mele, Phys. Rev. Lett. **95**, 146802 (2005).

[23] B. A. Bernevig, T. L. Hughes, and S. Zhang, Science **314**, 1757 (2006).

[24] L. Fu, C. L. Kane, and E. J. Mele, Phys. Rev. Lett. **98**, 106803 (2007).

[25] Y. Xia, D. Qian, D. Hsieh, L. Wray, A. Pal, H. Lin, A. Bansil, D. Grauer, Y. S. Hor, R. J. Cava, and M. Z. Hasan, Nat. Phys. **5**, 398 (2009).

[26] A. A. Taskin, H. F. Legg, F. Yang, S. Sasaki, Y. Kanai, K. Matsumoto, A. Rosch, and Y. Ando, Nat. Commun. **8**, 1340 (2017).

[27] A. Sulaev, M. Zeng, S.-Q. Shen, S.-K. Cho, W.-G. Zhu, Y.-P. Feng, S. V. Eremeev, Y. Kawazoe, L. Shen, and L. Wang, Nano Lett. **15**, 2061 (2015).

[28] A. Kandala, A. Richardella, S. Kempinger, C.-X. Liu, and N. Samarth, Nat. Commun. **6**, 7434 (2015).

[29] P. He, S. S.-L. Zhang, D.-P. Zhu, Y. Liu, Y. Wang, J.-W. Yu, G. Vignale, and H. Yang, Nat. Phys. **14**, 495 (2018).

[30] P. He, S. S.-L. Zhang, D.-P. Zhu, S.-Y. Shi, O. G. Heinonen, G. Vignale, and H. Yang, Phys. Rev. Lett. **123**, 016801 (2019).

[31] K. Yasuda, A. Tsukazaki, R. Yoshimi, K. S. Takahashi, M. Kawasaki, and Y. Tokura, Phys. Rev. Lett. **117**, 127202 (2016).

[32] K. Yasuda, A. Tsukazaki, R. Yoshimi, K. Kondou, K. S. Takahashi, Y. Otani, M. Kawasaki, and Y. Tokura, Phys. Rev. Lett. **119**, 137204 (2017).

[33] R. S. Akzyanov and A. L. Rakhmanov, Phys. Rev. B **97**, 075421 (2018).

[34] S. Nandy, A. Taraphder, and S. Tewari, Sci. Rep. **8**, 14983 (2018).

[35] A. Dyrdał, J. Barnaś, and A. Fert, Phys. Rev. Lett. **124**, 046802 (2020).

[36] X.-Q. Yu, Z.-G. Zhu, and G. Su, Phys. Rev. B **103**, 035410 (2021).

[37] A. G. Moghaddam, A. Qaiumzadeh, A. Dyrdal, and J. Berakdar, Phys. Rev. Lett. **125**, 196801 (2020).

[38] A. A. Zyuzin, M. D. Hook, and A. A. Burkov, Phys. Rev. B **83**, 245428 (2011).

[39] G. Zhang, H. Qin, J. Teng, J. Guo, Q. Guo, X. Dai, Z. Fang, and K. Wu, Appl. Phys. Lett. **95**, 053114 (2009).

[40] H. Peng, K. Lai, D. Kong, S. Meister, Y. Chen, X. Qi, S. Zhang, Z. Shen, and Y. Cui, Nat. Mater. **9**, 225 (2010).

[41] S.-Q. Shen, *Topological Insulators: Dirac Equation in Condensed Matters* (Springer, Berlin, 2012).

[42] C.-X. Liu, X.-L. Qi, H.-J. Zhang, X. Dai, Z. Fang, and S.-C. Zhang, Phys. Rev. B **82**, 045122 (2010).

[43] C. J. Tabert and J. P. Carbotte, Phys. Rev. B **91**, 235405 (2015).

[44] J. M. Ziman, *Electrons and Phonons :The Theory of Transport Phenomena in Solids* (Clarendon Press, Oxford, 2001).

[45] See Supplemental Material at http://link.aps.org/supplemental/10.1103/PhysRevB.103.155415 for details of the derivation of linear and nonlinear planar Hall effect in surface hybridized topological insulator thin films.

[46] T. Chiba, S. Takahashi, and G. E. W. Bauer, Phys. Rev. B **95**, 094428 (2017).

[47] M. Trushin, K. Vübornü, P. Moraczewski, A. A. Kovalev, J. Schliemann, and T. Jungwirth, Phys. Rev. B **80**, 134405 (2009).

[48] P. He, C.-H. Hsu, S.-Y. Shi, K.-M. Cai, J.-Y. Wang, Q.-S. Wang, G. Eda, H. Lin, V. M. Pereira, and H. Yang, Nat. Commun. **10**, 1290 (2019).

[49] S.-K. Chong, K.-B. Han, T. D. Sparks, and V. V. Deshpande, Phys. Rev. Lett. **123**, 036804 (2019).

[50] Y. Xu, I. Miotkowski, and Y.-P. Chen, Nat. Commun. **7**, 11434 (2016).